

EPRecon: An Efficient Framework for Real-Time Panoptic 3D Reconstruction from Monocular Video

Zhen Zhou^{1,2}, Yunkai Ma^{1,2}, Junfeng Fan¹, Shaolin Zhang¹, Fengshui Jing^{1,2,*}, and Min Tan^{1,2}

Abstract—Panoptic 3D reconstruction from a monocular video is a fundamental perceptual task in robotic scene understanding. However, existing efforts suffer from inefficiency in terms of inference speed and accuracy, limiting their practical applicability. We present EPRecon, an efficient real-time panoptic 3D reconstruction framework. Current volumetric-based reconstruction methods usually utilize multi-view depth map fusion to obtain scene depth priors, which is time-consuming and poses challenges to real-time scene reconstruction. To end this, we propose a lightweight module to directly estimate scene depth priors in a 3D volume for reconstruction quality improvement by generating occupancy probabilities of all voxels. In addition, to infer richer panoptic features from occupied voxels, EPRecon extracts panoptic features from both voxel features and corresponding image features, obtaining more detailed and comprehensive instance-level semantic information and achieving more accurate segmentation results. Experimental results on the ScanNetV2 dataset demonstrate the superiority of EPRecon over current state-of-the-art methods in terms of both panoptic 3D reconstruction quality and real-time inference. Code is available at <https://github.com/zhen6618/EPRecon>.

I. INTRODUCTION

Recently, visual-based panoptic 3D reconstruction [1] has gradually attracted attention due to its rich scene understanding information and wide application scenarios, such as robotic mapping and manipulation [2], and augmented reality (AR) [3]. Since camera poses can be accurately obtained by systems such as visual odometry [4], robot kinematics [5], or Simultaneous Localization and Mapping (SLAM) [6], [7], the main challenge in panoptic 3D reconstruction from a monocular video is how to obtain dense and high-quality scene surface depth from continuous RGB sequences and perform panoptic segmentation on the reconstructed scene.

Methods that fuse multi-view depth maps obtained from similarity matching along epipolar lines, such as MVSNet series [8]–[12], suffer from depth estimation inconsistencies and redundant computations. To end this, volumetric-based methods [1], [13]–[16] directly predict the explicit surface occupancy probabilities or implicit truncated signed distance function (TSDF) values to reconstruct scene surfaces in a 3D volume. To improve reconstruction quality, some works [1], [16], [17] first use off-the-shelf depth estimation models such

as monocular depth estimation [18] for a preliminary estimate of scene depth priors, which can eliminate the majority of non-surface voxels (over 90%), and then perform depth-guided reconstruction. Although these methods effectively improve reconstruction performance, the scene depth estimation networks used in existing methods are time-consuming, posing challenges to real-time scene reconstruction.

To simultaneously obtain panoptic segmentation information and depth information from image sequences, recent studies [1], [19] first predict occupancy probabilities of voxels, and then conduct 3D panoptic segmentation on predicted reconstructed voxels. Although these methods have shown certain efficacy, their panoptic features are only extracted from occupied voxel features or corresponding image features, resulting in limited instance-level semantic information. This is because voxel features need to generate rich geometric features for depth predictions and usually emphasize detailed semantic information. After multi-scale feature extraction and fusion, image features generally emphasize comprehensive semantic information.

In this paper, we propose EPRecon, an efficient real-time panoptic 3D reconstruction framework. We first estimate scene depth priors in a 3D volume to eliminate most of non-surface voxels, and then perform depth-guided panoptic 3D reconstruction. Unlike previous works [1], [16], [17] which directly use time-consuming depth estimation models to obtain 2D depth priors and then perform depth fusion, EPRecon introduces a lightweight module to directly estimate scene depth priors in a 3D volume by generating occupancy probabilities of all voxels. Specifically, EPRecon back-projects multi-view image features into the volume and extracts feature similarities between views. These features are further aggregated and converted into occupancy probabilities of voxels. The module makes EPRecon focus more on voxel feature extraction in regions near scene surfaces and improves the entire panoptic reconstruction quality.

Subsequently, to recover dense and coherent panoptic reconstruction results, EPRecon follows the workflow of previous studies [1], [14] to predict surface occupancy probabilities and TSDF values in a coarse-to-fine manner. Then, 3D panoptic segmentation is performed on the predicted occupied voxels. Different from current methods [1], [19] that extract panoptic features only from occupied voxel features or corresponding image features, we extract panoptic features from both types of features, obtaining more detailed and comprehensive panoptic segmentation information. We use a deformable cross-attention module [20] to fuse them. Voxel features make local segmentation regions more detailed and

This work was supported by the National Natural Science Foundation of China (62173327, 62373354), the Beijing Natural Science Foundation (4232057), and the Youth Innovation Promotion Association of CAS (2022130).

¹The authors are with the State Key Laboratory of Multimodal Artificial Intelligence Systems, Institute of Automation, Chinese Academy of Sciences, Beijing, 100190, China. ²The authors are with the School of Artificial Intelligence, University of Chinese Academy of Sciences, Beijing, 100049, China. * Corresponding author. fengshui.jing@ia.ac.cn

image features make global understanding more comprehensive. The efficient design of EPrecon makes panoptic 3D reconstruction more coherent and reasonable, while also featuring real-time inference. The main contributions are summarized as follows.

- We propose EPrecon, an efficient real-time panoptic 3D reconstruction framework, which outperforms state-of-the-art (SOTA) methods in terms of both panoptic 3D reconstruction quality and real-time inference.
- We introduce a lightweight module to directly estimate scene depth priors in a 3D volume, which eliminates the majority of non-surface voxels and improves panoptic reconstruction quality.
- We extract panoptic features from voxel features and corresponding image features, obtaining more detailed and comprehensive panoptic segmentation information and achieving more accurate segmentation results.

II. RELATED WORK

A. 3D Geometry Reconstruction

3D reconstruction from RGB image sequences has a long research history, and many classic works have emerged, such as MVSNet [8] and ORB-SLAM3 [6]. Multi-view stereo reconstruction methods represented by MVSNet series [8]–[12] estimate depth map for each view and then perform depth map fusion. These methods greatly improve the accuracy of 3D reconstruction, however, multiple depth estimations from different views suffer from depth estimation inconsistencies and redundant computations, usually generating artifacts and repeated surfaces. Volumetric-based approaches [13]–[15], [21]–[25] directly predict surface occupancy probabilities or TSDF values in a 3D volume. An early work is Atlas [13], which directly regressed a TSDF volume from a set of posed RGB images. NeuralRecon [14] reconstructed local surfaces represented by sparse TSDF volumes for each video fragment sequentially, and used GRUs to fuse TSDF volumes. To achieve more detailed reconstruction, recent studies [1], [16], [17], [26], [27] first estimate scene depth priors and then perform depth-guided scene reconstruction. For example, DG-Recon [26] utilized multi-view depth priors to eliminate many irrelevant non-surface voxels and guide surface reconstruction. FineRecon [27] combined depth priors and global image features for surface occupancy predictions. PanoRecon [1] performed panoptic reconstruction with the guidance of MVS depth estimation. Although a preliminary estimate of the scene depth can recover more accurate surfaces, the depth prior prediction modules in existing methods are time-consuming, posing challenges to real-time panoptic reconstruction. To end this, we propose a lightweight module to directly estimate scene depth priors in the 3D volume.

B. 3D Panoptic Segmentation

3D panoptic segmentation is mainly performed on voxel features or point features. Previous studies [28]–[34] mainly integrate the results of semantic segmentation and instance

segmentation branches to obtain the final panoptic segmentation results. For example, PANet [28] combined semantic predictions generated by a semantic head and detected instances generated by an instance aggregation module to infer panoptic segmentation predictions. Recently, compared to panoptic segmentation methods based on group voting or clustering [1], [35], [36], mask transformer-based methods [37], [38] demonstrate impressive performance by establishing query decoders to directly generate masks for “thing” classes and “stuff” classes. MaskPLS [37] used multiple decoder layers to process learnable queries and point features for generating masks and semantic classes. Mask4Former [38] applied the mask transformer framework to 4D panoptic segmentation. Inspired by the competitive performance of the mask transformer framework, we apply this powerful framework for 3D panoptic segmentation without hand-crafted non-learned association strategies.

C. Panoptic 3D Reconstruction

A more challenging task is to perform panoptic 3D reconstruction on RGB image sequences. Some video panoptic segmentation approaches such as PVO [39], VPSNet [40] and ViP-DeepLab [41] can generate depth predictions. With panoptic segmentation, [42] predicted panoptic maps based on ORB-SLAM2 [43]. However, these methods mainly focus on performing accurate panoptic segmentation on images and exhibit segmentation inconsistencies and limited performance in 3D space. To improve the quality of 3D panoptic segmentation, recent studies [1], [19] directly conduct panoptic segmentation on predicted reconstructed voxels. PanoRecon [1] utilized a semantic prediction branch and an offset prediction branch for the predicted occupied voxel features to generate the semantic class and instance center shift vector of each voxel, respectively. Then, the outputs of the two branches were sent to the instance detection module to obtain instance objects. Based on the mask transformer framework [44], SparseOcc [19] queried the image features corresponding to predicted occupied voxels and predicted the masks of “thing” classes and “stuff” classes. Panoptic-FlashOcc [45] extracted panoptic features from bird’s-eye-view (BEV) voxel features. However, their panoptic features are only extracted from voxel features or corresponding image features, which have limited instance-level semantic information. Our method also uses the mask transformer framework and fuses both types of features, achieving more detailed and comprehensive panoptic segmentation results.

D. Neural Radiance Fields and 3D Gaussian Splatting

Recently, self-supervised learning-based approaches are developed. Neural Radiance Fields (NeRF) [46]–[48] series and 3D Gaussian Splatting (3DGS) [49] series generate high-quality panoptic segmentation results from novel perspectives while also recovering scene depth information. Although NeRF and 3DGS methods exhibit remarkable performance in scene rendering and understanding, they primarily focus on novel view synthesis, having limited capability in depth information acquisition and usually suffering from noise,

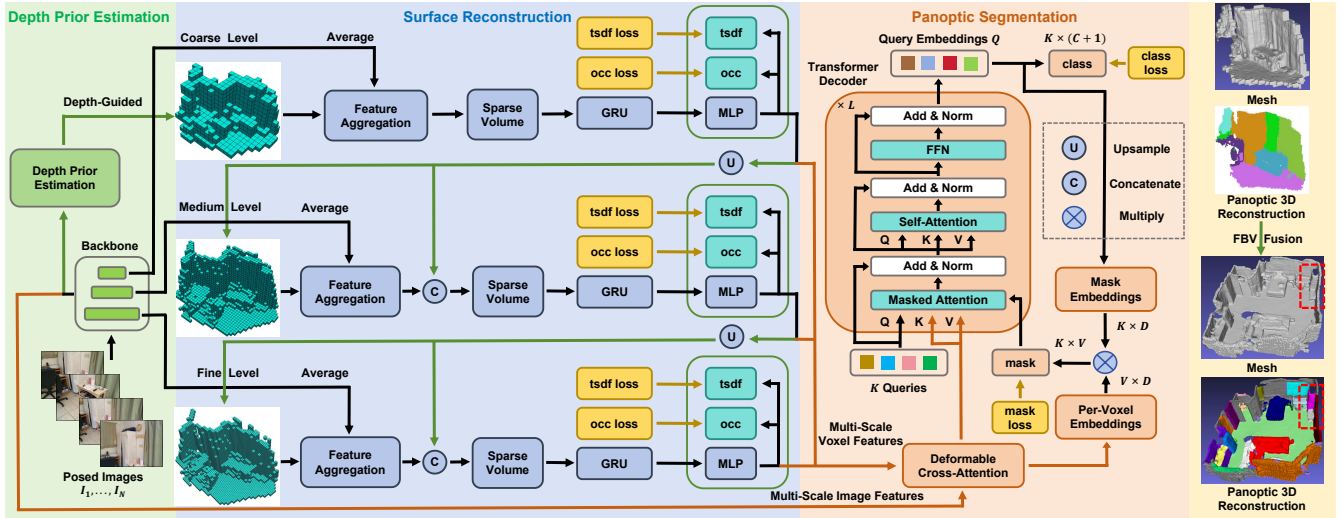


Fig. 1. Architecture of the proposed EPRecon. EPRecon directly estimates scene depth priors in a 3D volume, and then performs depth-guided panoptic reconstruction. To obtain depth information, we predict the surface occupancy probabilities and TSDF values of voxels. Panoptic features are extracted from both voxel features and corresponding image features, obtaining more detailed and comprehensive instance-level semantic information. EPRecon performs panoptic reconstruction within each FBV and gradually recovers the entire scene in chronological order (see the rightmost column for visualization results).

artifacts, and missing details. Our proposed method focuses more on recovering high-quality scene depth and is directly supervised by depth information.

III. METHODS

A. Overview

Given a sequence of monocular images $\{I_t\}$ as input, where the intrinsic parameters $\{K_t\}$ and extrinsic parameters $\{P_t\}$ are obtained by systems such as SLAM [6] systems, EPRecon aims to reconstruct dense and coherent 3D surfaces from these posed images, while simultaneously performing panoptic segmentation on the reconstructed scene surfaces.

To provide enough motion parallax and keep multi-view co-visibility for panoptic reconstruction, following the training strategy of [14], a frame is selected as a key frame if its relative translation is greater than t_{\max} and the relative rotation angle is greater than R_{\max} . A window with N key frames is defined as a local fragment, and the global panoptic reconstruction result is fused from all local fragments. The maximum visible depth of each view is set to d_{\max} , and all view frustums in a fragment are limited to a cubic-shaped and voxelized fragment bounding volume (FBV, $\mathcal{B} \in \mathbb{R}^{B \times B \times B}$). EPRecon is mainly conducted within each FBV, and its overall flowchart is depicted as in Fig. 1. It consists of three major stages: depth prior estimation, surface reconstruction, and panoptic segmentation.

B. Depth Prior Estimation

EPRecon introduces a lightweight module, which is shown in Fig. 2, to directly estimate the scene depth priors in the current FBV \mathcal{B}_t . Motivated by the principle that the pixel features of each view corresponding to the same voxel in the FBV are similar, we determine whether a voxel is located on scene surfaces based on the similarities between the corresponding pixel features. Given N key frame images $\{I_1, \dots, I_N\}$, EPRecon first utilizes a backbone to extract

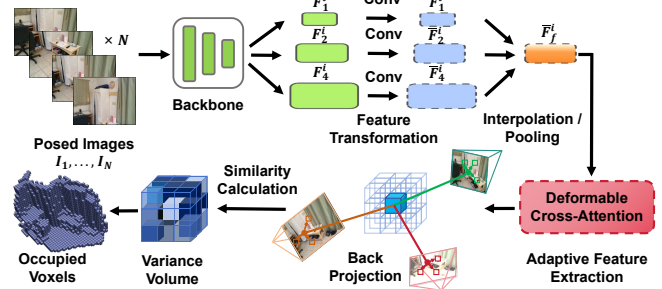


Fig. 2. Illustration of the proposed depth prior estimation module.

multi-scale image features for each view. The image features at three scales $\{\mathcal{F}_1^i, \mathcal{F}_2^i, \mathcal{F}_4^i\}$ are extracted for further processing, where the numbers represent relative multiples of feature map resolution and i is the image index. To further highlight the differences between different pixel features, $\{\mathcal{F}_1^i, \mathcal{F}_2^i, \mathcal{F}_4^i\}$ are converted into features $\{\bar{\mathcal{F}}_1^i, \bar{\mathcal{F}}_2^i, \bar{\mathcal{F}}_4^i\}$ representing pixel similarity via a convolution-based transformation module. Subsequently, we merge $\{\bar{\mathcal{F}}_1^i, \bar{\mathcal{F}}_2^i, \bar{\mathcal{F}}_4^i\}$ into one scale using interpolation and pooling operations, obtaining $\bar{\mathcal{F}}_f^i$.

After capturing the pixel features of all views, these pixel features are back-projected into the corresponding voxels in the FBV \mathcal{B}_t according to the camera's intrinsic parameters $\{K_t\}$ and extrinsic parameters $\{P_t\}$. However, for each voxel, only obtaining the features of one pixel in each view for similarity calculation is not robust enough, and selecting pixel features within a window introduces interference pixels. To address this problem, we adaptively select the features of multiple pixels around each pixel as the features of that pixel, which improves robustness and reduces interference pixels. Specifically, a deformable cross-attention module is applied to adaptively extract pixel features. For each voxel \mathcal{V}_i in the FBV \mathcal{B}_t , EPRecon extracts the pixel features $\{p_1, \dots, p_N\}$ ($p_i \in \mathbb{R}^C$, C is the feature dimension) of N corresponding views via back-projection.

Then, we use variance to represent feature similarity across all views. For pixels projected outside the view boundaries, they are not involved in the variance calculation to reduce similarity calculation errors. Hence, the feature mean $\mu_v \in \mathbb{R}^C$ of each voxel is calculated as

$$\mu_v = \frac{m_1 p_1 + m_2 p_2 + \dots + m_N p_N}{m_1 + m_2 + \dots + m_N}, \quad m_i \in \{0, 1\}, \quad (1)$$

where m_i indicates whether a voxel \mathcal{V}_i is correctly projected within the view boundary. The corresponding variance $\sigma_v^2 \in \mathbb{R}^C$ is formulated as

$$\sigma_v^2 = \frac{m_1(p_1 - \mu_v)^2 + m_2(p_2 - \mu_v)^2 + \dots + m_N(p_N - \mu_v)^2}{m_1 + m_2 + \dots + m_N}. \quad (2)$$

The variances of all voxels form a variance volume Σ_v . The advantage of using variance is that its calculation is independent of the number of correctly projected views $\sum m_i$. This allows voxels with fewer correctly projected views to calculate similarities accurately, and voxels with more correctly projected views to enhance the robustness of similarity calculation.

Subsequently, sparse 3D convolutions are applied to further aggregate the features in the variance volume Σ_v , followed by a simple Multi-Layer Perceptron (MLP) for transforming variances into surface occupancy probabilities \mathcal{O}_v . We use continuous $1-|\text{TSDF}|$ ($1 - |\mathcal{T}_v|$, $\mathcal{T}_v \in [-1, 1]$) values as the supervised targets for the predicted surface occupancy probabilities. The log-transformed L1 distance loss is used as the loss function

$$\mathcal{L}_D = \frac{1}{B^3} \sum_{i=1}^{B^3} |\log(\sigma(\mathcal{O}_v) + 1) - \log(2 - |\mathcal{T}_v|)|. \quad (3)$$

Voxels with a surface occupancy probability greater than a predefined threshold are selected as occupied voxels. Then, we select the occupied voxels as the initial voxels for panoptic reconstruction, which has eliminated the majority of non-surface voxels.

C. Surface Reconstruction

Inspired by previous works [1], [14], we gradually recover the scene surfaces in a coarse-to-fine manner. Image features from different views are back-projected into occupied voxels, and the average pixel features are taken as the features of the occupied voxels. These voxels with view-agnostic features form a 3D sparse volume, and 3D submanifold sparse convolutions [50] are used for further feature extraction, which maintains the geometric structure of the volume.

Subsequently, to maintain temporal coherence and consistency between fragments, the voxel features and corresponding image features of the previous FBV \mathcal{B}_{t-1} are merged into the current FBV \mathcal{B}_t . Following [14], a 3D convolutional variant of the Gated Recurrent Unit (GRU) [51] module is applied for temporal fusion.

Finally, surface occupancy probabilities and TSDF values of all voxels in the current volume are predicted via a simple MLP module. Voxels with a surface occupancy probability

greater than a predefined threshold are selected as final occupied voxels. Marching Cubes algorithm [52] is performed on the TSDF values within the predicted occupied voxels to reconstruct the scene mesh and obtain more granular depth.

For supervision, occupancy losses and TSDF losses at all the coarse-to-fine levels have the same definition forms. The occupancy loss \mathcal{L}_O is defined as the binary cross-entropy (BCE) loss between the predicted surface occupancy probabilities \mathcal{O}_r and the ground-truth surface occupancy probabilities \mathcal{O}_r^{gt} , which is formulated as

$$\mathcal{L}_O = -[\mathcal{O}_r^{gt} \log \sigma(\mathcal{O}_r) + (1 - \mathcal{O}_r^{gt}) \log \sigma(1 - \mathcal{O}_r)]. \quad (4)$$

The TSDF loss \mathcal{L}_T is defined as the L1 distance loss between the log-transformed predicted TSDF values \mathcal{T}_r and the log-transformed ground-truth TSDF values \mathcal{T}_r^{gt} .

$$\mathcal{L}_T = |\text{sgn}(\mathcal{T}_r) \log(|\mathcal{T}_r| + 1) - \text{sgn}(\mathcal{T}_r^{gt}) \log(|\mathcal{T}_r^{gt}| + 1)|, \quad (5)$$

where $\text{sgn}(\cdot)$ is the sign function.

D. Panoptic Segmentation

Panoptic segmentation is performed on the final predicted occupied voxels. Inspired by the mask transformer framework [44], [53], EPRecon performs feature queries to occupied voxels, generating a binary mask for each “thing” or “stuff” class. As voxel features are primarily used for recovering surface geometry, they usually focus more on local geometric structures and more detailed semantic information. Image features excel at capturing more comprehensive semantic information across multiple scales. To recover more detailed and comprehensive panoptic segmentation results, the panoptic features of the occupied voxels are extracted from both voxel features and corresponding image features. To extract richer instance-level semantic information, we first map the occupied voxels predicted at the fine level back to the coarse and medium levels to obtain multi-scale voxel features and corresponding image features. Then, similar to the depth prior estimation module, we use a deformable cross-attention module to fuse voxel features and corresponding image features separately at each scale.

Given K queries and fused multi-scale features \mathcal{F}_p , a transformer decoder attends to \mathcal{F}_p and produces K per-segment query embeddings \mathcal{Q}_p . In the transformer decoder, there are L repeated transformer blocks, each consisting of a masked cross-attention module, a self-attention module, and a feed-forward network (FFN). Cross-attention associates each query with a “thing”, “stuff” or empty class. Specifically, the masked attention mechanism limits the attention range to the foreground region of the prediction mask of each query, improving interaction efficiency and reducing memory usage. We use Fourier positional encodings [54] based on voxel positions. Self-attention understands and distinguishes different queries. Subsequently, the K produced query embeddings \mathcal{Q}_p independently generate K class predictions with K corresponding mask embeddings $\mathcal{Q}_p^m \in \mathbb{R}^{K \times D}$ (D is the feature dimension). These mask embeddings \mathcal{Q}_p^m are then dot-producted with per-voxel embeddings $\mathcal{V}_p^m \in \mathbb{R}^{V \times D}$

(V is the number of occupied voxels) extracted from \mathcal{F}_p to generate K binary masks $\mathcal{M}_p^m \in \mathbb{R}^{K \times V}$, where $\mathcal{M}_p^m = \mathcal{Q}_p^m(\mathcal{V}_p^m)^T$. Then, the predicted masks are used for masked cross-attention in the next transformer block and inference of the final panoptic segmentation results.

Following [53], an auxiliary loss is added to every intermediate transformer block and to the learnable query features before the transformer decoder. We use BCE loss and dice loss [55] for the mask loss \mathcal{L}_M , and cross-entropy (CE) loss for the classification loss \mathcal{L}_C . The weighted sum of losses from all modules constitutes the final loss

$$\mathcal{L}_{\text{all}} = \lambda_D \mathcal{L}_D + \lambda_O \mathcal{L}_O + \lambda_T \mathcal{L}_T + \lambda_M \mathcal{L}_M + \lambda_C \mathcal{L}_C, \quad (6)$$

where $\{\lambda_D, \lambda_O, \lambda_T, \lambda_M, \lambda_C\}$ are weights.

E. Implementation Details

For the training strategy, we first train the lightweight depth prior estimation module for 24 epochs. Then, we freeze the network weights in the depth prior estimation module, and train the remaining panoptic reconstruction modules for 200 epochs. The entire network is trained on a single NVIDIA Tesla A800 GPU for 14 days. The voxel sizes from coarse to fine levels in the surface reconstruction module are set to 16cm, 8cm, and 4cm, respectively. TSDF truncation distance is 12cm, and d_{max} is set to 3m. Nearest-neighbor interpolation is used in the upsampling operations between coarse-to-fine levels. R_{max} and t_{max} are set to 15° and 0.1m, respectively. We set 9 views as the length of a fragment. We use 6 transformer blocks with 80 queries in the transformer decoder by default. The loss weights $\{\lambda_D, \lambda_O, \lambda_T, \lambda_M, \lambda_C\}$ are set to $\{0.5, 1.0, 1.0, 0.6, 0.24\}$. For instance fusion across different FBVs, we consider instances with the same semantic label to be the same instance if the IoU (Intersection over Union) between them exceeds 0.05.

IV. EXPERIMENTS

A. Dataset

We conduct panoptic 3D reconstruction experiments on ScanNet(V2) [56], which is a large and richly-annotated dataset with RGB images, camera poses, surface reconstruction annotations, and instance-level semantic segmentation annotations. The training set, validation set and test set contain 1201, 312 and 100 scenes, respectively. It contains more than 2,500,000 frames. For fair comparison, we use the official dataset split for training and evaluation. All RGB images are resized to 640×480 .

B. Comparisons with the State-of-the-Art

We first conduct comparison experiments on the test set to demonstrate the superiority of EPRecon over current SOTA methods. The experimental results of other methods and metric calculation are borrowed from [1].

1) *3D Geometry Reconstruction*: We follow the 3D geometry metrics used in [1], [14] to evaluate the 3D geometry reconstruction performance of our proposed EPRecon. The experimental results are shown in Table I. Our EPRecon is an online geometry reconstruction method and outperforms

TABLE I
QUANTITATIVE RESULTS OF 3D GEOMETRY RECONSTRUCTION. † INDICATES USING DEPTH MAP FUSION. THE BEST RESULTS ARE HIGHLIGHTED IN BLUE, ORANGE, AND PURPLE, RESPECTIVELY

Method	Online	Comp↓	Acc↓	Recall†	Prec†	F-score†
MVDNet† [9]	-	4.0	24.0	0.831	0.208	0.329
DPSNet† [57]	-	4.5	28.4	0.793	0.223	0.344
GPMVS† [58]	-	10.5	19.1	0.423	0.339	0.373
SimRec† [18]	-	6.2	10.1	0.636	0.536	0.577
Atlas [13]	✗	8.3	10.1	0.566	0.600	0.579
Vortex [23]	✗	8.1	6.2	0.605	0.689	0.643
NeuRec [14]	✓	13.7	5.6	0.470	0.678	0.553
Zuo et al. [17]	✓	11.0	5.8	0.505	0.665	0.572
PanoRec [1]	✓	8.9	6.4	0.530	0.656	0.584
EPRecon	✓	10.2	5.1	0.519	0.692	0.593

TABLE II
QUANTITATIVE RESULTS OF 3D SEMANTIC SEGMENTATION

Method	with Depth	Online	mIoU†
ScanNet [56]	✓	-	30.6
PointNet++ [59]	✓	-	33.9
SPLATNet [60]	✓	-	39.3
3DMV [61]	✓	-	48.4
SegFusion [62]	✓	-	51.5
PanopticFusion [3]	✓	-	52.9
SparseConvNet [63]	✓	-	72.5
MinkowskiNet [64]	✓	-	73.4
Atlas [13]	✗	✗	34.0
PanoRecon [1]	✗	✓	52.4
EPRecon	✗	✓	54.7

existing online volumetric-based methods and depth map fusion-based methods in terms of the ‘‘F-score’’ metric, which demonstrates that EPRecon has achieved a better balance between the reconstruction accuracy and completeness. Especially, with the assistance of the proposed depth prior estimation module, EPRecon achieves a higher ‘‘precision’’ metric than all depth map fusion-based methods and volumetric-based methods, recovering more accurate and concise geometric surfaces. The ‘‘recall’’ metric of EPRecon is slightly lower than PanoRecon because EPRecon does not generate excessive redundant geometric structures due to depth map fusion used for depth prior estimation.

2) *3D Panoptic Segmentation*: Following [1], we evaluate the 3D semantic segmentation performance in Table II and 3D instance segmentation performance in Table III. For a comprehensive evaluation, we also compare with methods that utilize depth information as input. Despite the unfair setting since we only use RGB data, EPRecon is still surprisingly competitive with (or even outperforms) some previous studies that use 3D input data. Moreover, compared with methods that only take 2D image data as input, our method achieves the best semantic segmentation performance of 54.7% mIoU, and the best instance segmentation performance of 25.8% AP50 and 51.6% AP25. Compared with PanoRecon, which simultaneously generates both geometric and instance-level semantic information from voxel features, EPRecon obtains richer panoptic features from both voxel features and corresponding image features. Furthermore, both PanoRecon and our method are online incremental

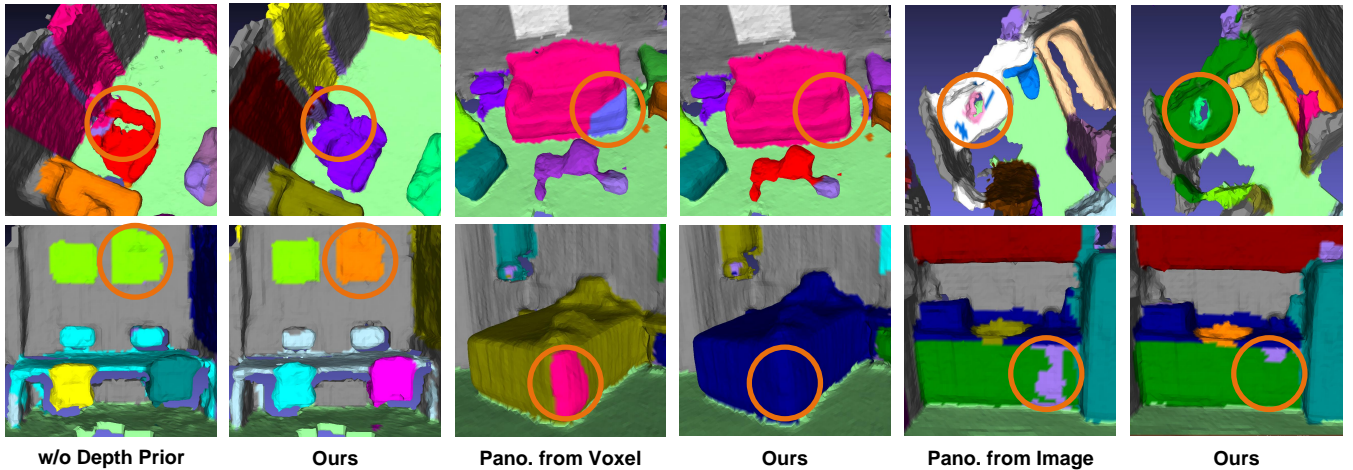


Fig. 3. Ablation study results of panoptic 3D reconstruction. Under the guidance of the proposed depth prior estimation module, EPRecon recovers more complete and accurate panoptic reconstruction results. Extracting panoptic-related features only from voxel features results in insufficient understanding of more comprehensive instance-level semantic information. Relying only on image features leads to insufficient capture of more detailed information.

TABLE III
QUANTITATIVE RESULTS OF 3D INSTANCE SEGMENTATION

Method	with Depth	Online	AP50 \uparrow	AP25 \uparrow
SGPN [65]	✓	-	0.143	0.390
ASIS [66]	✓	-	0.199	0.422
Gspn [67]	✓	-	0.306	0.544
3D-SIS [65]	✓	-	0.382	0.558
SegGroup [68]	✓	-	0.445	0.637
PBNet [69]	✓	-	0.747	0.825
Mask3D [54]	✓	-	0.780	0.870
PanoRecon [1]	✗	✓	0.227	0.484
EPRecon	✗	✓	0.258	0.516

reconstruction methods and cannot directly obtain global panoptic features, which further demonstrates the superior performance of EPRecon.

3) *Runtime Analysis*: For fair comparison, we perform runtime evaluation on a single NVIDIA RTX3090 GPU. Since PanoRecon first introduces the task of panoptic 3D reconstruction from a posed monocular video, we mainly compare our work with it. As shown in Table IV, each fragment contains 9 key frames, and we give the average inference time for each fragment. Thanks to the lightweight depth prior estimation module, the inference speed of EPRecon is significantly faster than PanoRecon, and EPRecon also achieves higher panoptic 3D reconstruction quality. EPRecon achieves a real-time panoptic 3D reconstruction speed of 31.36 KFPS (key frames per second), which is 2.4 \times faster than PanoRecon.

C. Ablation Studies

In Table V, we conduct ablation studies to verify the effectiveness of the components in EPRecon. The qualitative comparison and analysis are shown in Fig. 3. The proposed depth prior estimation module effectively improves the quality of 3D geometric reconstruction and 3D panoptic segmentation. Since we directly estimate scene depth priors in a 3D volume, our proposed module is more lightweight (13.4 \times faster) than current depth prior estimation methods

TABLE IV
RUNTIME ANALYSIS OF PANOPTIC 3D RECONSTRUCTION

Method	Depth Prior Estimation	Panoptic 3D Reconstruction	Runtime
PanoRecon [1]	430 ms	700 ms	12.85 KFPS
EPRecon	32 ms	287 ms	31.36 KFPS

TABLE V
ABLATION STUDIES ON THE SCANNET(V2) VALIDATION SET

Method	Recall	Prec	F-score	mIoU	AP50	AP25
w/o Depth Prior	0.524	0.681	0.592	55.0	0.265	0.515
Pano. from Voxel	0.548	0.694	0.612	55.5	0.269	0.520
Pano. from Image	0.567	0.700	0.626	55.8	0.273	0.524
Ours	0.575	0.709	0.635	56.3	0.289	0.531

based on depth map fusion (see Table IV). In addition, we compare with extracting panoptic features only from voxel features or corresponding image features. Our method captures both types of features, having more detailed and comprehensive instance-level semantic information, which leads to higher 3D panoptic segmentation performance.

V. CONCLUSION

In this work, we propose EPRecon, an efficient real-time panoptic 3D reconstruction framework. In EPRecon, a lightweight module is introduced to directly estimate scene depth priors in a 3D volume, eliminating the majority of non-surface voxels and improving panoptic reconstruction quality. Additionally, we extract panoptic features from both voxel features and corresponding image features, obtaining more detailed and comprehensive panoptic segmentation information. Experimental results demonstrate the superiority of EPRecon over SOTA methods in terms of panoptic reconstruction quality and real-time inference. The limitations are that the model training time is long and the non-learning-based instance fusion method between FBVs is not efficient. Future work will focus on improvements in these aspects.

REFERENCES

- [1] D. Wu, Z. Yan, and H. Zha, "Panorecon: Real-time panoptic 3d reconstruction from monocular video," in *IEEE Conference on Computer Vision and Pattern Recognition*, June 2024, pp. 21 507–21 518.
- [2] M. Han, Z. Zhang, Z. Jiao, X. Xie, Y. Zhu, S.-C. Zhu, and H. Liu, "Reconstructing interactive 3d scenes by panoptic mapping and cad model alignments," in *IEEE International Conference on Robotics and Automation*, 2021, pp. 12 199–12 206.
- [3] G. Narita, T. Seno, T. Ishikawa, and Y. Kaji, "Panopticfusion: Online volumetric semantic mapping at the level of stuff and things," in *IEEE/RSJ International Conference on Intelligent Robots and Systems*, 2019, pp. 4205–4212.
- [4] M. He, C. Zhu, Q. Huang, B. Ren, and J. Liu, "A review of monocular visual odometry," in *The Visual Computer*, vol. 36, no. 5, May 2020, pp. 1053–1065.
- [5] J. Jiang, X. Luo, Q. Luo, L. Qiao, and M. Li, "An overview of hand-eye calibration," *International Journal of Advanced Manufacturing Technology*, vol. 119, no. 1, pp. 77–97, Mar 2022.
- [6] C. Campos, R. Elvira, J. J. G. Rodríguez, J. M. M. Montiel, and J. D. Tardós, "Orb-slam3: An accurate open-source library for visual, visual-inertial, and multimap slam," *IEEE Transactions on Robotics*, vol. 37, no. 6, pp. 1874–1890, 2021.
- [7] C.-M. Chung, Y.-C. Tseng, Y.-C. Hsu, X.-Q. Shi, Y.-H. Hua, J.-F. Yeh, W.-C. Chen, Y.-T. Chen, and W. H. Hsu, "Orbeez-slam: A real-time monocular visual slam with orb features and nerf-realized mapping," in *IEEE International Conference on Robotics and Automation*, 2023, pp. 9400–9406.
- [8] Y. Yao, Z. Luo, S. Li, T. Fang, and L. Quan, "Mvsnet: Depth inference for unstructured multi-view stereo," in *European Conference on Computer Vision*, September 2018.
- [9] K. Wang and S. Shen, "Mvdepthnet: Real-time multiview depth estimation neural network," in *International Conference on 3D Vision*, 2018, pp. 248–257.
- [10] Y. Yao, Z. Luo, S. Li, T. Shen, T. Fang, and L. Quan, "Recurrent mvsnet for high-resolution multi-view stereo depth inference," in *IEEE Conference on Computer Vision and Pattern Recognition*, June 2019.
- [11] X. Gu, Z. Fan, S. Zhu, Z. Dai, F. Tan, and P. Tan, "Cascade cost volume for high-resolution multi-view stereo and stereo matching," in *IEEE Conference on Computer Vision and Pattern Recognition*, June 2020.
- [12] Z. Yu and S. Gao, "Fast-mvsnet: Sparse-to-dense multi-view stereo with learned propagation and gauss-newton refinement," in *IEEE Conference on Computer Vision and Pattern Recognition*, June 2020.
- [13] Z. Murez, T. van As, J. Bartolozzi, A. Sinha, V. Badrinarayanan, and A. Rabinovich, "Atlas: End-to-end 3d scene reconstruction from posed images," in *European Conference on Computer Vision*, 2020, pp. 414–431.
- [14] J. Sun, Y. Xie, L. Chen, X. Zhou, and H. Bao, "Neuralrecon: Real-time coherent 3d reconstruction from monocular video," in *IEEE Conference on Computer Vision and Pattern Recognition*, June 2021, pp. 15 598–15 607.
- [15] A. Bozic, P. Palafox, J. Thies, A. Dai, and M. Niessner, "Transformerfusion: Monocular rgb scene reconstruction using transformers," in *Advances in Neural Information Processing Systems*, vol. 34, 2021, pp. 1403–1414.
- [16] Y. Li, Z. Yu, C. Choy, C. Xiao, J. M. Alvarez, S. Fidler, C. Feng, and A. Anandkumar, "Voxformer: Sparse voxel transformer for camera-based 3d semantic scene completion," in *IEEE Conference on Computer Vision and Pattern Recognition*, June 2023, pp. 9087–9098.
- [17] X. Zuo, N. Yang, N. Merrill, B. Xu, and S. Leutenegger, "Incremental dense reconstruction from monocular video with guided sparse feature volume fusion," *IEEE Robotics and Automation Letters*, vol. 8, no. 6, pp. 3876–3883, 2023.
- [18] M. Sayed, J. Gibson, J. Watson, V. Prisacariu, M. Firman, and C. Godard, "Simplerecon: 3d reconstruction without 3d convolutions," in *European Conference on Computer Vision*, 2022, pp. 1–19.
- [19] H. Liu, H. Wang, Y. Chen, Z. Yang, J. Zeng, L. Chen, and L. Wang, "Fully sparse 3d panoptic occupancy prediction," *arXiv preprint arXiv:2312.17118*, 2023.
- [20] X. Zhu, W. Su, L. Lu, B. Li, X. Wang, and J. Dai, "Deformable detr: Deformable transformers for end-to-end object detection," *International Conference on Learning Representations*, 2021.
- [21] W. Yuan, X. Gu, H. Li, Z. Dong, and S. Zhu, "3d-former: Monocular scene reconstruction with 3d sdf transformers," in *International Conference on Learning Representations*, 2023.
- [22] Z. Feng, L. Yang, P. Guo, and B. Li, "Cvrecon: Rethinking 3d geometric feature learning for neural reconstruction," in *IEEE International Conference on Computer Vision*, October 2023, pp. 17 750–17 760.
- [23] N. Stier, A. Rich, P. Sen, and T. Höllerer, "Vortex: Volumetric 3d reconstruction with transformers for voxelwise view selection and fusion," in *International Conference on 3D Vision*, 2021, pp. 320–330.
- [24] X. Wang, Z. Zhu, W. Xu, Y. Zhang, Y. Wei, X. Chi, Y. Ye, D. Du, J. Lu, and X. Wang, "Openoccupancy: A large scale benchmark for surrounding semantic occupancy perception," in *IEEE International Conference on Computer Vision*, October 2023, pp. 17 850–17 859.
- [25] H. Gao, Y. Liu, F. Cao, H. Wu, F. Xu, and S. Zhong, "Vidar: Data quality improvement for monocular 3d reconstruction through in-situ visual interaction," in *IEEE International Conference on Robotics and Automation*, 2024, pp. 7895–7901.
- [26] J. Ju, C. W. Tseng, O. Bailo, G. Dikov, and M. Ghafoorian, "Dg-recon: Depth-guided neural 3d scene reconstruction," in *IEEE International Conference on Computer Vision*, October 2023, pp. 18 184–18 194.
- [27] N. Stier, A. Ranjan, A. Colburn, Y. Yan, L. Yang, F. Ma, and B. Angles, "Finerecon: Depth-aware feed-forward network for detailed 3d reconstruction," in *IEEE International Conference on Computer Vision*, October 2023, pp. 18 423–18 432.
- [28] J. Mei, Y. Yang, M. Wang, X. Hou, L. Li, and Y. Liu, "Panet: Lidar panoptic segmentation with sparse instance proposal and aggregation," in *IEEE/RSJ International Conference on Intelligent Robots and Systems*, 2023, pp. 7726–7733.
- [29] F. Hong, L. Kong, H. Zhou, X. Zhu, H. Li, and Z. Liu, "Unified 3d and 4d panoptic segmentation via dynamic shifting networks," *IEEE Transactions on Pattern Analysis and Machine Intelligence*, vol. 46, no. 5, pp. 3480–3495, 2024.
- [30] J. Behley, A. Milioto, and C. Stachniss, "A benchmark for lidar-based panoptic segmentation based on kitti," in *IEEE International Conference on Robotics and Automation*, 2021, pp. 13 596–13 603.
- [31] S. Xu, R. Wan, M. Ye, X. Zou, and T. Cao, "Sparse cross-scale attention network for efficient lidar panoptic segmentation," *AAAI Conference on Artificial Intelligence*, vol. 36, no. 3, pp. 2920–2928, Jun. 2022.
- [32] J. Li, X. He, Y. Wen, Y. Gao, X. Cheng, and D. Zhang, "Panoptic-phnet: Towards real-time and high-precision lidar panoptic segmentation via clustering pseudo heatmap," in *IEEE Conference on Computer Vision and Pattern Recognition*, June 2022, pp. 11 809–11 818.
- [33] R. Razani, R. Cheng, E. Li, E. Taghavi, Y. Ren, and L. Bingbing, "Gp-s3net: Graph-based panoptic sparse semantic segmentation network," in *IEEE International Conference on Computer Vision*, October 2021, pp. 16 076–16 085.
- [34] D. Ye, Z. Zhou, W. Chen, Y. Xie, Y. Wang, P. Wang, and H. Foroosh, "Lidarmultinet: Towards a unified multi-task network for lidar perception," *AAAI Conference on Artificial Intelligence*, vol. 37, no. 3, pp. 3231–3240, Jun. 2023.
- [35] F. Hong, L. Kong, H. Zhou, X. Zhu, H. Li, and Z. Liu, "Unified 3d and 4d panoptic segmentation via dynamic shifting networks," *IEEE Transactions on Pattern Analysis and Machine Intelligence*, vol. 46, no. 5, pp. 3480–3495, 2024.
- [36] Z. Zhang, Z. Zhang, Q. Yu, R. Yi, Y. Xie, and L. Ma, "Lidar-camera panoptic segmentation via geometry-consistent and semantic-aware alignment," in *IEEE International Conference on Computer Vision*, October 2023, pp. 3662–3671.
- [37] R. Marcuzzi, L. Nunes, L. Wiesmann, J. Behley, and C. Stachniss, "Mask-based panoptic lidar segmentation for autonomous driving," *IEEE Robotics and Automation Letters*, vol. 8, no. 2, pp. 1141–1148, 2023.
- [38] K. Yilmaz, J. Schult, A. Nekrasov, and B. Leibe, "Mask4former: Mask transformer for 4d panoptic segmentation," in *IEEE International Conference on Robotics and Automation*, 2024, pp. 9418–9425.
- [39] W. Ye, X. Lan, S. Chen, Y. Ming, X. Yu, H. Bao, Z. Cui, and G. Zhang, "Pvo: Panoptic visual odometry," in *IEEE Conference on Computer Vision and Pattern Recognition*, June 2023, pp. 9579–9589.
- [40] D. Kim, S. Woo, J.-Y. Lee, and I. S. Kweon, "Video panoptic segmentation," in *IEEE Conference on Computer Vision and Pattern Recognition*, June 2020.
- [41] S. Qiao, Y. Zhu, H. Adam, A. Yuille, and L.-C. Chen, "Vip-deeplab: Learning visual perception with depth-aware video panoptic segmentation," in *IEEE Conference on Computer Vision and Pattern Recognition*, June 2021, pp. 3997–4008.

- [42] H. Zhu, C. Yao, Z. Zhu, Z. Liu, and Z. Jia, "Fusing panoptic segmentation and geometry information for robust visual slam in dynamic environments," in *IEEE International Conference on Automation Science and Engineering*, 2022, pp. 1648–1653.
- [43] R. Mur-Artal and J. D. Tardós, "Orb-slam2: An open-source slam system for monocular, stereo, and rgb-d cameras," *IEEE Transactions on Robotics*, vol. 33, no. 5, pp. 1255–1262, 2017.
- [44] B. Cheng, A. Schwing, and A. Kirillov, "Per-pixel classification is not all you need for semantic segmentation," in *Advances in Neural Information Processing Systems*, vol. 34, 2021, pp. 17 864–17 875.
- [45] Z. Yu, C. Shu, Q. Sun, J. Linghu, X. Wei, J. Yu, Z. Liu, D. Yang, H. Li, and Y. Chen, "Panoptic-flashocc: An efficient baseline to marry semantic occupancy with panoptic via instance center," in *arXiv preprint arXiv:2406.10527*, 2024.
- [46] X. Fu, S. Zhang, T. Chen, Y. Lu, L. Zhu, X. Zhou, A. Geiger, and Y. Liao, "Panoptic nerf: 3d-to-2d label transfer for panoptic urban scene segmentation," in *International Conference on 3D Vision*, 2022, pp. 1–11.
- [47] A. Kundu, K. Genova, X. Yin, A. Fathi, C. Pantofaru, L. J. Guibas, A. Tagliasacchi, F. Dellaert, and T. Funkhouser, "Panoptic neural fields: A semantic object-aware neural scene representation," in *IEEE Conference on Computer Vision and Pattern Recognition*, June 2022, pp. 12 871–12 881.
- [48] C. Smitt, M. Halstead, P. Zimmer, T. Läbe, E. Guclu, C. Stachniss, and C. McCool, "Pag-nerf: Towards fast and efficient end-to-end panoptic 3d representations for agricultural robotics," *IEEE Robotics and Automation Letters*, vol. 9, no. 1, pp. 907–914, 2024.
- [49] B. Dou, T. Zhang, Y. Ma, Z. Wang, and Z. Yuan, "Cosseggaussians: Compact and swift scene segmenting 3d gaussians with dual feature fusion," *arXiv preprint arXiv:2401.05925*, 2024.
- [50] S. Contributors, "Spconv: Spatially sparse convolution library," <https://github.com/traveller59/spconv>, 2022.
- [51] J. Chung, C. Gulcehre, K. Cho, and Y. Bengio, "Empirical evaluation of gated recurrent neural networks on sequence modeling," *arXiv preprint arXiv:1412.3555*, 2014.
- [52] W. E. Lorensen and H. E. Cline, "Marching cubes: A high resolution 3d surface construction algorithm," in *SIGGRAPH*, 1987, pp. 163–169.
- [53] B. Cheng, I. Misra, A. G. Schwing, A. Kirillov, and R. Girdhar, "Masked-attention mask transformer for universal image segmentation," in *IEEE Conference on Computer Vision and Pattern Recognition*, June 2022, pp. 1290–1299.
- [54] J. Schult, F. Engelmann, A. Hermans, O. Litany, S. Tang, and B. Leibe, "Mask3d: Mask transformer for 3d semantic instance segmentation," in *IEEE International Conference on Robotics and Automation*, 2023, pp. 8216–8223.
- [55] F. Milletari, N. Navab, and S.-A. Ahmadi, "V-net: Fully convolutional neural networks for volumetric medical image segmentation," in *International Conference on 3D Vision*, 2016, pp. 565–571.
- [56] A. Dai, A. X. Chang, M. Savva, M. Halber, T. Funkhouser, and M. Niessner, "Scannet: Richly-annotated 3d reconstructions of indoor scenes," in *IEEE Conference on Computer Vision and Pattern Recognition*, July 2017.
- [57] S. Im, H.-G. Jeon, S. Lin, and I. S. Kweon, "Dpsnet: End-to-end deep plane sweep stereo," in *arXiv preprint arXiv:1905.00538*, 2019.
- [58] Y. Hou, J. Kannala, and A. Solin, "Multi-view stereo by temporal nonparametric fusion," in *IEEE International Conference on Computer Vision*, October 2019.
- [59] C. R. Qi, L. Yi, H. Su, and L. J. Guibas, "Pointnet++: Deep hierarchical feature learning on point sets in a metric space," in *Advances in Neural Information Processing Systems*, vol. 30, 2017.
- [60] H. Su, V. Jampani, D. Sun, S. Maji, E. Kalogerakis, M.-H. Yang, and J. Kautz, "Splatnet: Sparse lattice networks for point cloud processing," in *IEEE Conference on Computer Vision and Pattern Recognition*, June 2018.
- [61] A. Dai and M. Niessner, "3dmv: Joint 3d-multi-view prediction for 3d semantic scene segmentation," in *European Conference on Computer Vision*, September 2018.
- [62] D. Menini, S. Kumar, M. R. Oswald, E. Sandström, C. Sminchisescu, and L. Van Gool, "A real-time online learning framework for joint 3d reconstruction and semantic segmentation of indoor scenes," *IEEE Robotics and Automation Letters*, vol. 7, no. 2, pp. 1332–1339, 2022.
- [63] B. Graham, M. Engelcke, and L. van der Maaten, "3d semantic segmentation with submanifold sparse convolutional networks," in *IEEE Conference on Computer Vision and Pattern Recognition*, June 2018.
- [64] C. Choy, J. Gwak, and S. Savarese, "4d spatio-temporal convnets: Minkowski convolutional neural networks," in *IEEE Conference on Computer Vision and Pattern Recognition*, June 2019.
- [65] W. Wang, R. Yu, Q. Huang, and U. Neumann, "Sgpn: Similarity group proposal network for 3d point cloud instance segmentation," in *IEEE Conference on Computer Vision and Pattern Recognition*, June 2018.
- [66] X. Wang, S. Liu, X. Shen, C. Shen, and J. Jia, "Associatively segmenting instances and semantics in point clouds," in *IEEE Conference on Computer Vision and Pattern Recognition*, June 2019.
- [67] L. Yi, W. Zhao, H. Wang, M. Sung, and L. J. Guibas, "Gspn: Generative shape proposal network for 3d instance segmentation in point cloud," in *IEEE Conference on Computer Vision and Pattern Recognition*, June 2019.
- [68] A. Tao, Y. Duan, Y. Wei, J. Lu, and J. Zhou, "Seggroup: Seg-level supervision for 3d instance and semantic segmentation," *IEEE Transactions on Image Processing*, vol. 31, pp. 4952–4965, 2022.
- [69] W. Zhao, Y. Yan, C. Yang, J. Ye, X. Yang, and K. Huang, "Divide and conquer: 3d point cloud instance segmentation with point-wise binarization," in *IEEE International Conference on Computer Vision*, October 2023, pp. 562–571.